From Reaction Cone to Catastrophe: Unveiling the Kinetic Chain of Thermal Runaway within Li-Ion Batteries (Tsinghua, JEC, IF 15.6)

Source: En·Sim SGer (Simulation & Energy Storage)
Original Paper Link: https://doi.org/10.1016/j.jechem.2026.07.094

Journal of Energy Chemistry

Date: Available online 24 August 2026

In Press, Journal Pre-proof

Research article • Full text access Get rights and content

From reaction cone to catastrophe: Unveiling the kinetic chain of thermal runaway within Li-ion batteries

Fangshu Zhang [a], Xuning Feng [a], Enhong Liu [b], Yifan Wang [a], Wei Xiao [c], Changyong Jin [a], Yong Peng [a], Chengshan Xu [a], Li Wang [d], Xiangming He [d], Minggao Ouyang [a]

[a] State Key Laboratory of Intelligent Green Vehicle and Mobility, Tsinghua University, Beijing 100084, China
[b] College of Engineering, China Agricultural University, Beijing 100083, China
[c] School of Mechatronic Engineering, Yangtze University, Jingzhou 434022, Hubei, China
[d] Institute of Nuclear and New Energy Technology, Tsinghua University, Beijing 100084, China

Received 8 May 2026, Revised 18 July 2026, Accepted 31 July 2026, Available online 24 August 2026.

What do these dates mean?

Research Content

1.1 Scientific Question

The spatiotemporal coupling mechanism among localized internal short circuits, multi-front evolution, and progressive material failure during propagation of the internal thermal-runaway front (TRF).

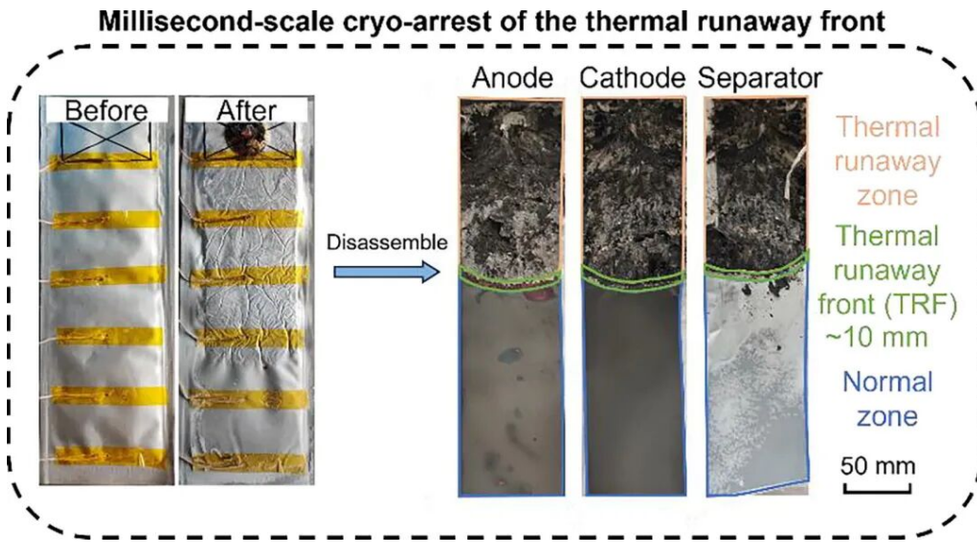

1.2 Methods

1.2.1Cell Parameters 点击箭头弹出图

Table 1. Battery parameters.

Parameter	Description
Mass	590 g
Geometry	Length × Width × Height = 292 mm × 76 mm × 11 mm
Nominal capacity	57 Ah
Nominal voltage	2.7–4.2 V
Nominal charging current	1/3 C
Cathode	$LiNi_{0.8}Co_{0.1}Mn_{0.1}O_2$
Initial state of charge	Nominally 100% SOC
Anode	Graphite
Energy density	357.46 Wh kg^{-1}

Key parameters of the tested cell.

1.2.2 Theoretical Analysis: TR Reaction Cone and the Cryogenic Arrest Strategy

(1) TR Reaction Cone Model (Fig. 1)

Formation mechanism: A localized internal short circuit generates heat, raising the local temperature from ambient T∞ up to the trigger temperature T2; exothermic reactions further raise it to the peak T3.

Reaction-cone definition: The thermochemically active region formed by coupling of chemical reactions, heat transfer, and mass transport is defined as the TR reaction cone; its spatial expansion corresponds to TRF propagation.

Propagation mechanism: Heat generated at the reaction-cone center diffuses outward, driving the TRF to propagate outward at velocity vTR.

Arrest criterion: When vTR = 0, the TRF stops. This is essentially governed by the competition between internal heat generation and external heat dissipation.

Key parameters: TRF propagation is jointly governed by QV, λ, ρ, Cp, h, and the geometric heat-dissipation factor S*.

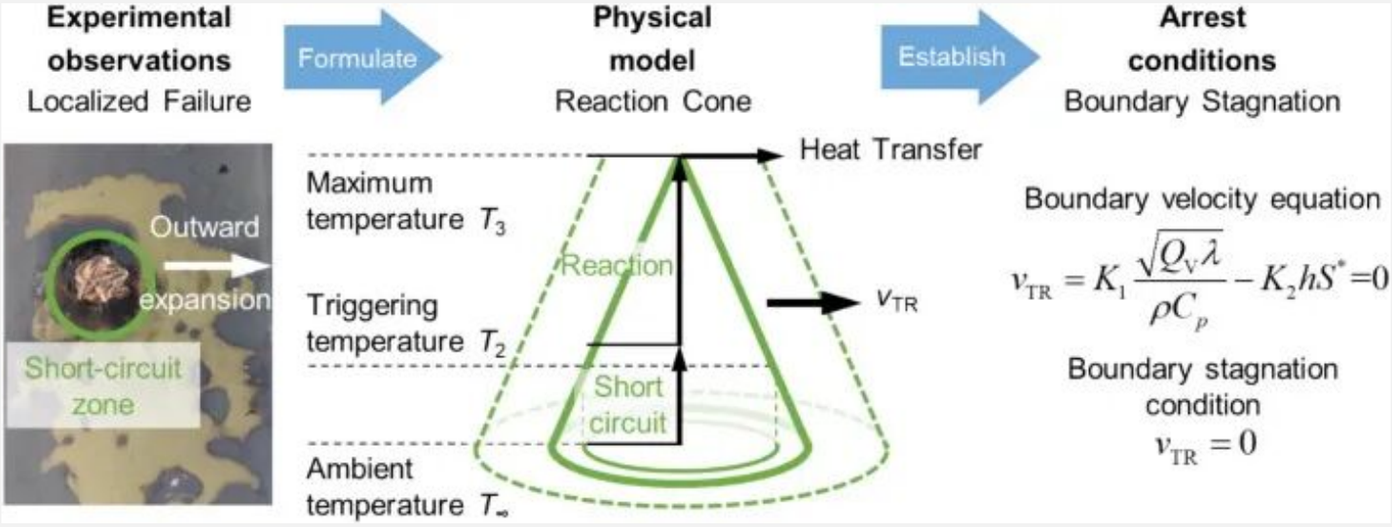

Fig. 1. Thermal runaway front: initiation, propagation, and arrest.

(2) TRF Suppression Strategies (Fig. 2)

Chemical suppression: Raise T1 and T2, lower T3 and the volumetric heat-generation rate QV — weakening the exothermic reaction at its source and reducing the reaction-cone height.

Physical suppression: Lower the thermal conductivity λ, raise the density ρ and specific heat Cp — weakening internal thermal diffusion and limiting the spatial expansion of the reaction cone.

Enhanced heat dissipation: Raise the effective heat-transfer coefficient h and the geometric heat-dissipation factor S* — strengthening external heat removal so the TRF gradually loses its self-sustaining propagation condition.

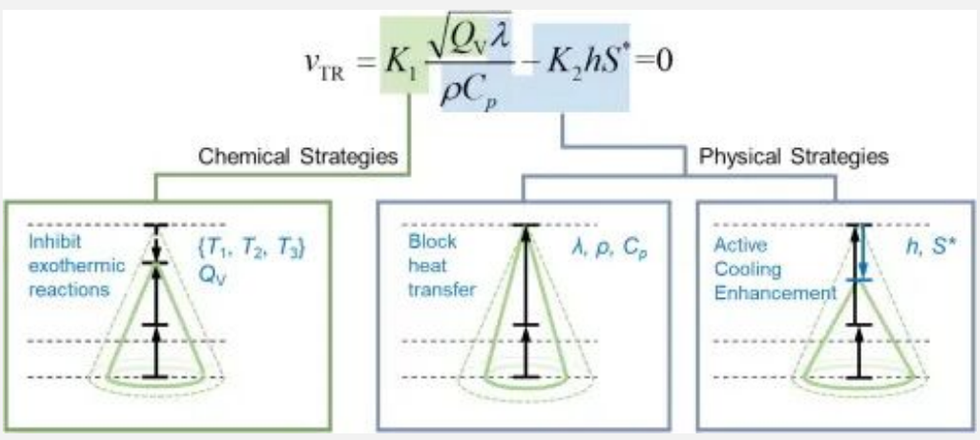

Fig. 2. TRF suppression conditions, including chemical and physical strategies.

(3) Liquid-Nitrogen Cryogenic Arrest Strategy (Fig. 3)

Triggering stage:TR is triggered at the cell top by induction heating; the TRF propagates downward at velocity vTR.

Cooling stage: The cell bottom is immersed in liquid nitrogen; intense boiling heat transfer lowers the heating rate and the TR peak temperature.

Freezing stage:As the TRF propagates downward, the heat-exchange area between the cell and liquid nitrogen continuously increases, and the cooling capacity keeps strengthening.

Arrest mechanism: When the heat released by the exothermic reaction is insufficient to sustain further TRF propagation, the TRF is arrested by cryogenic cooling.

Experimental significance: Liquid-nitrogen-enhanced cooling rapidly freezes the instantaneous structure of the TRF, providing an experimental basis for further resolving the internal reaction zone of the TRF.

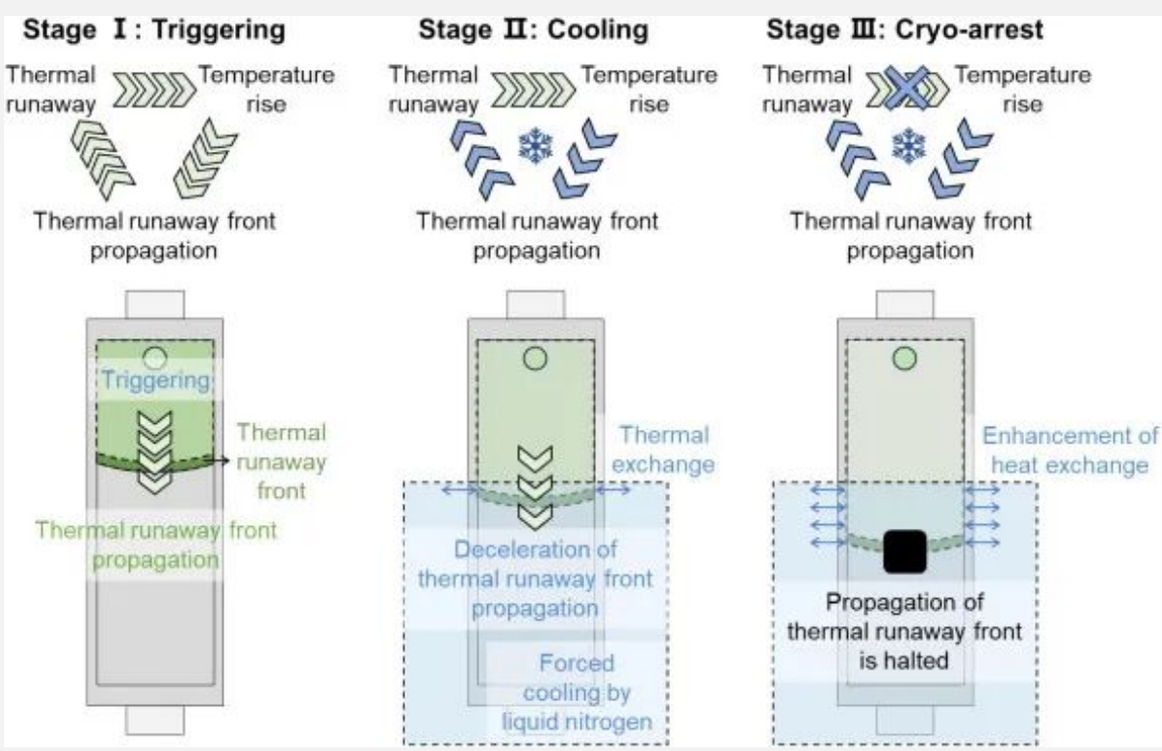

Fig. 3. Cryo-arrest mechanism of TRF: triggering, cooling, and cryo-arrest

1.2.3 In-situ Propagation Freezing Experiment of the Thermal Runaway Front

① Experimental setup (Fig. 4a)

Sample module: The cell is fixed by metal clamps to reduce the air gap between the cell and the aluminum-laminated film, improving cooling efficiency.

Loading module: Secures the sample and vertically transports it into the liquid-nitrogen bath.

Triggering module: Inductively heats the cell surface locally to trigger thermal runaway.

Cryogenic freezing module: Provides a stable liquid-nitrogen environment for rapid cooling and freezing of the TRF.

② Sample preparation (Fig. 4b–c)

Cell thickness is adjusted according to the cryogenic-freezing conditions; the original cell is disassembled in an argon glovebox and the corresponding electrode stack is extracted.

Re-encapsulated and heat-sealed with aluminum-laminated film to prepare thin cell samples.

The sample is fixed by metal clamps and bolts; guide holes ensure accurate alignment of the induction coil with the trigger position.

③ Experimental procedure (Fig. 4d)

The sample module is mounted on the loading module, and liquid nitrogen is injected into the cryogenic chamber.

The sample descends into the liquid nitrogen to an immersion depth of 192 mm, with a transport time of 40 s.

The induction coil moves to the cell surface and triggers top thermal runaway at 1.2 kW for 1 s.

After formation, the TRF propagates toward the cell bottom at vTR.

④ TRF freezing mechanism

As the TRF propagates downward, the contact area between the cell and liquid nitrogen continuously increases, and heat-dissipation capacity keeps strengthening.

When the temperature of the TRF leading edge drops below the thermal-runaway trigger temperature, the reaction can no longer be self-sustained, and the TRF is successfully arrested by cryogenic cooling.

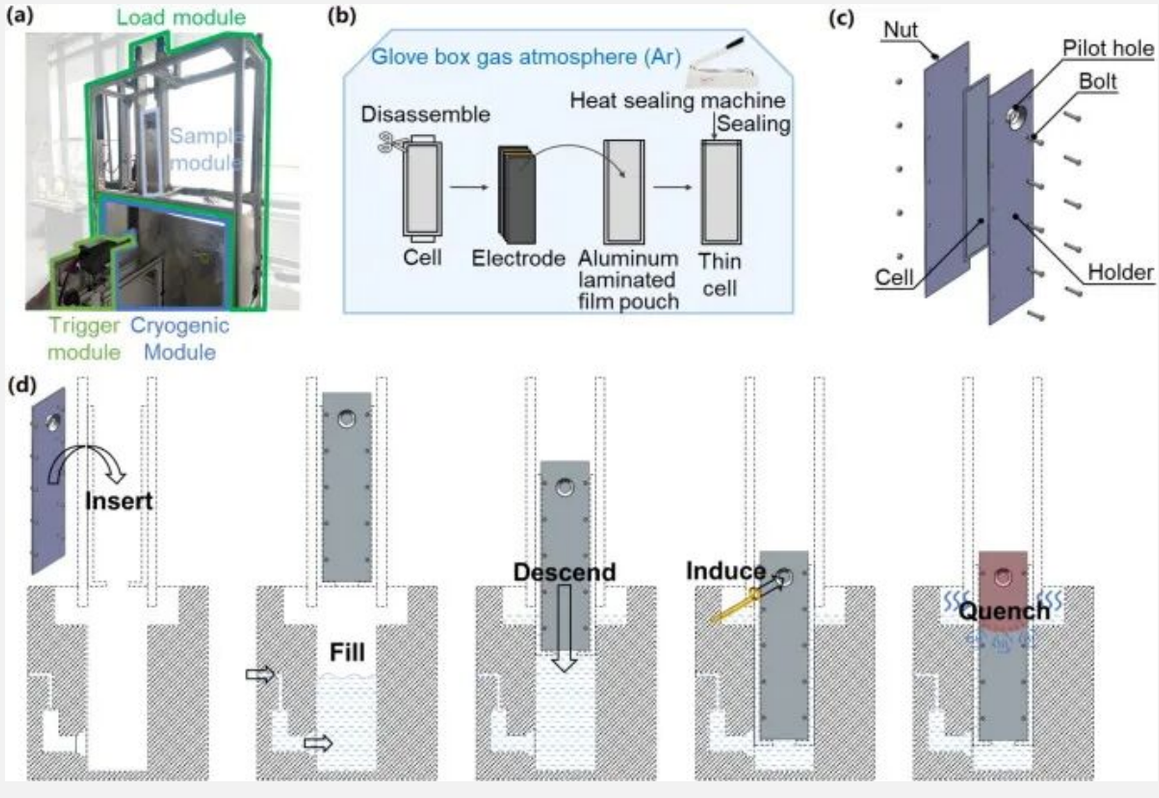

Table 2. Cryo-arrest condition parameters.

Symbol	Description	Value	Unit
d	Thickness of the cell	0.001	m
h	Equivalent convective heat transfer coefficient under liquid nitrogen immersion	1000	$W\ m^{-2}\ K^{-1}$
T_2	The triggering temperature of TR	200	°C

T_3	The maximum temperature of TR	1000	°C
T_∞	Ambient temperature	−196	°C
ρ	Density of the cell	2500	kg m^{-3}
C_p	Specific heat capacity of the cell	1000	J kg^{-1} K^{-1}
x_0	Length of TR area	0.1	m
v_{TR}	TRF velocity under liquid nitrogen cooling	0.01	m s^{-1}
Q_V	Volumetric heat generation rate	3.102×10^9	W m^{-3}

Fig. 4. Cryo-arrest device and cryo-arrest protocol for TRF

1.3 Results

4.3.1 Temperature and Cryo-Arrest Distance Analysis (Fig. 5)

Appearance changes (Fig. 5a): Before the experiment, the aluminum-laminated-film surface is flat and intact; after the experiment, obvious wrinkles appear in the TR-triggered region, while the non-TR region remains flat. The boundary between the wrinkled and flat regions can approximately characterize the TRF position.

Thermocouple arrangement (Fig. 5a): The top 40 mm of the cell is defined as the TR trigger zone; TC1 is placed at the center of the bottom of the trigger zone, and the remaining thermocouples are arranged along the propagation direction at 50 mm intervals to monitor TRF propagation.

Temperature response (Fig. 5b): Rapid cooling during liquid-nitrogen immersion causes thermocouple signal fluctuations; after TR triggering, TC1, TC2, TC3 and TC4 show successive temperature rises, while TC5 shows no obvious rise — indicating the TRF ultimately stops between TC4 and TC5.

Arrest-position determination: Combining thermocouple temperature changes, the aluminum-laminated-film wrinkle boundary, and the transition boundary between the reacted and unreacted regions after disassembly, the TRF arrest position is cross-validated.

0.1637 m	0.0222 m	13.6 %
Mean cryo-arrest distance (n = 15)	Standard deviation	Coefficient of variation (CV)

The CV of 13.6% indicates acceptable experimental scatter in the TRF arrest distance; the liquid-nitrogen cryo-arrest method can control the TRF stopping position stably and repeatably (measurement error ≈ ±10 ³ m).

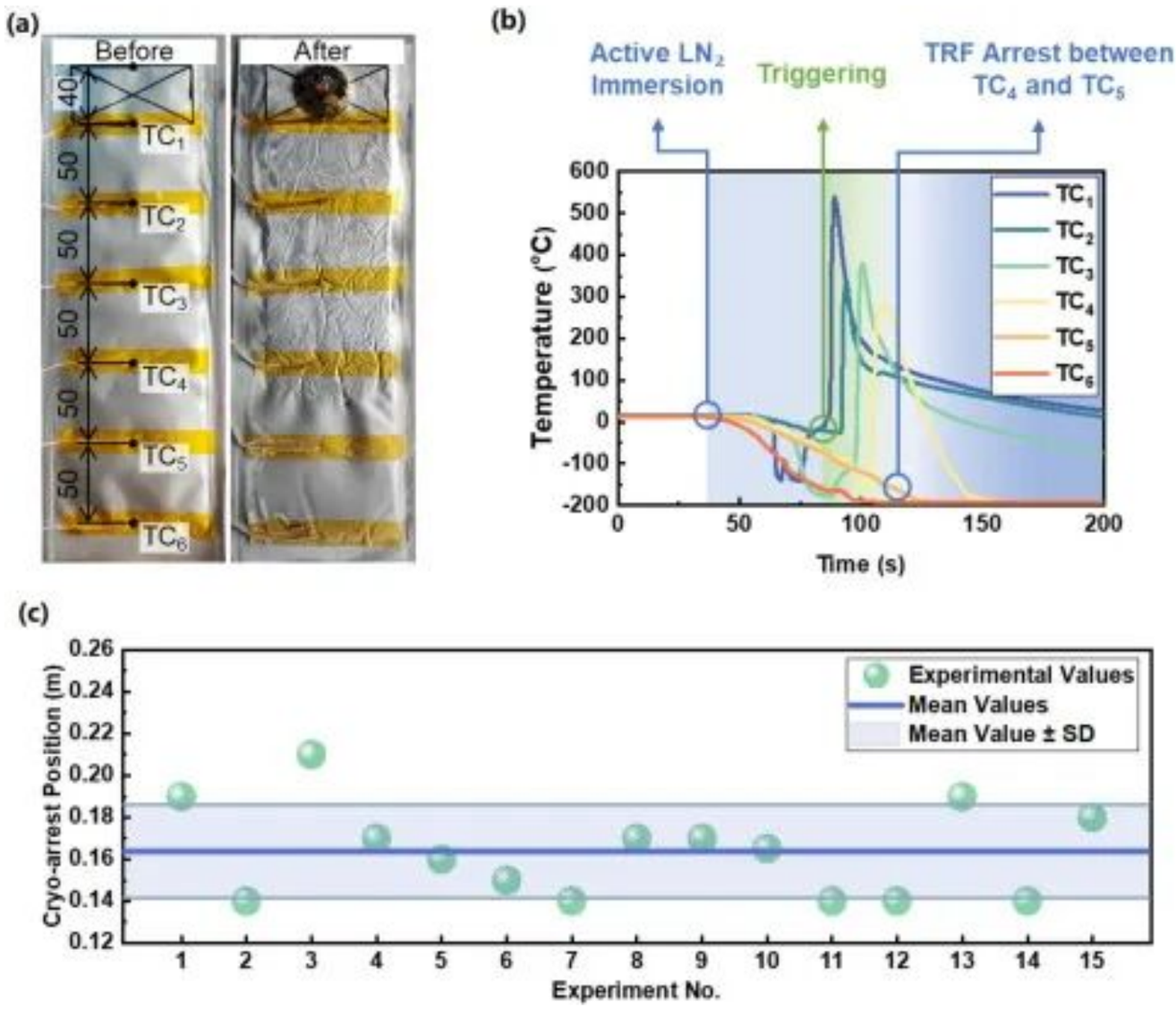

Fig. 5. TRF cryo-arrest data.

1.3.2 Morphology Tracking of the Thermal Runaway Front (Fig. 6)

Region division (Fig. 6a):The positive electrode, negative electrode, and separator debris clearly distinguish the TR region from the normal region; the transition region between them corresponds to the TRF, with a width of about 10 mm.

Internal short-circuit features (Fig. 6a): A distinct golden-yellow region appears on the negative electrode near the TRF, indicating separator failure induced a localized internal short circuit; the resulting short-circuit heat is one of the important heat sources driving further TRF propagation.

Electrode state changes (Fig. 6a): In the incompletely reacted region, the negative electrode gradually changes from a fully charged state to a discharged state, while the external negative electrode far from the TRF remains golden-yellow — further indicating that short-circuit discharge is closely related to TRF propagation.

Structural damage in the TR region (Fig. 6a–b): Because the NCM811 positive electrode has a high energy density, reactions in the TR region are intense; the positive electrode, negative electrode, and separator severely melt and fuse, making further optical differentiation difficult.

Separator and Al current-collector melting (Fig. 6b):The failed separator adheres to the negative-electrode surface, with a large number of molten aluminum beads on its surface, indicating TR high temperatures melted the aluminum current collector, and some molten aluminum may further participate in the TR reaction.

Multi-front propagation features (Fig. 6c): The TRF does not always propagate as a single arc-shaped front, but is formed by the superposition of multiple irregular arc-shaped local fronts.

TRF formation mechanism (Fig. 6d):Local TR first forms multiple arc-shaped fronts expanding outward from local reaction centers; when the propagation speeds of the fronts are close, their superimposed morphology approaches a circle.

Stable propagation stage (Fig. 6d): As propagation continues, different local fronts gradually merge, ultimately forming a relatively stable single arc-shaped TRF that continues to advance toward the unreacted region.

Mechanistic significance

The TRF evolves as "**local initiation → multi-front superposition→ front merging → stable propagation.**" This multi-front mechanism must be taken into account in subsequent TRF propagation models.

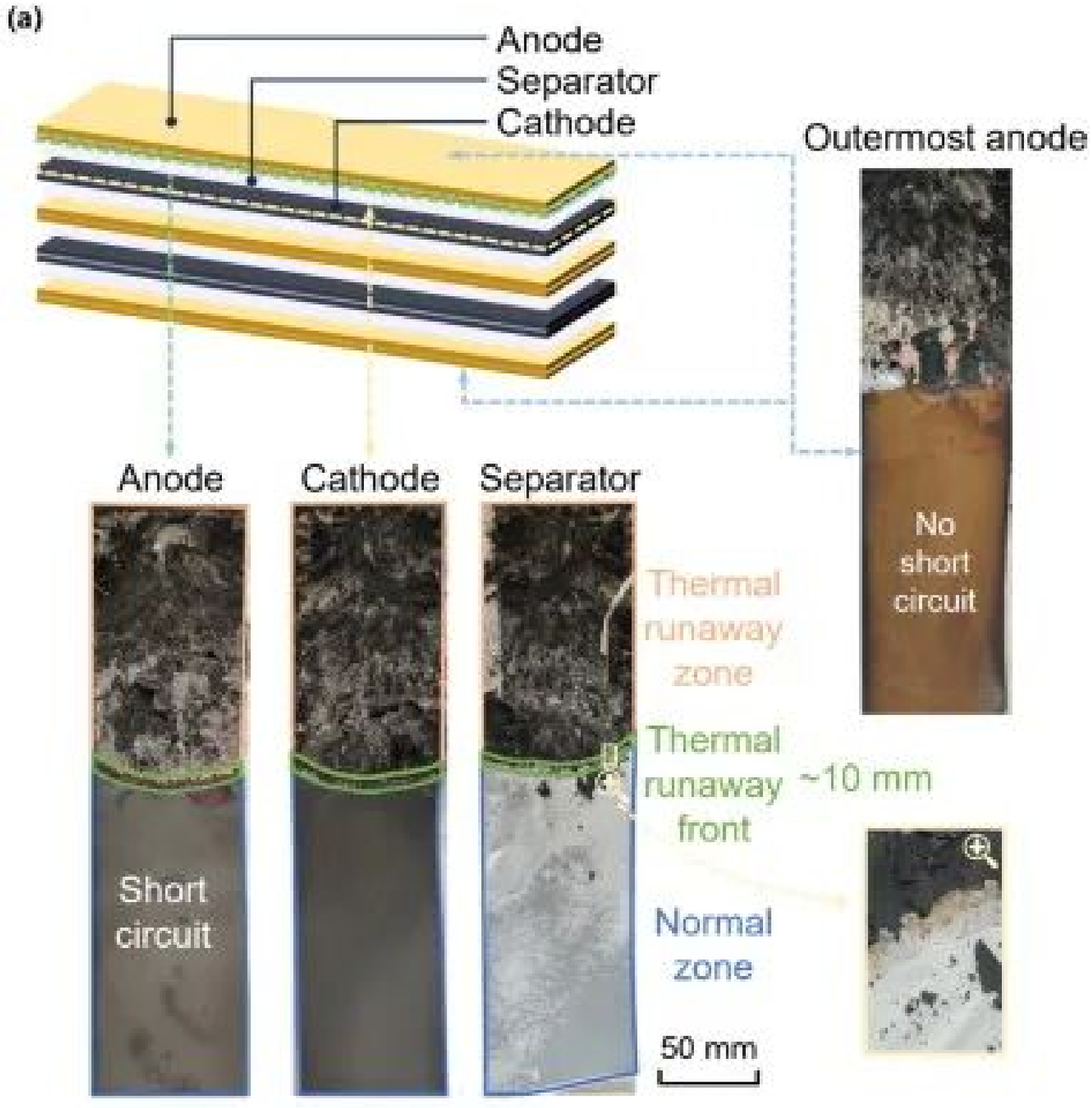

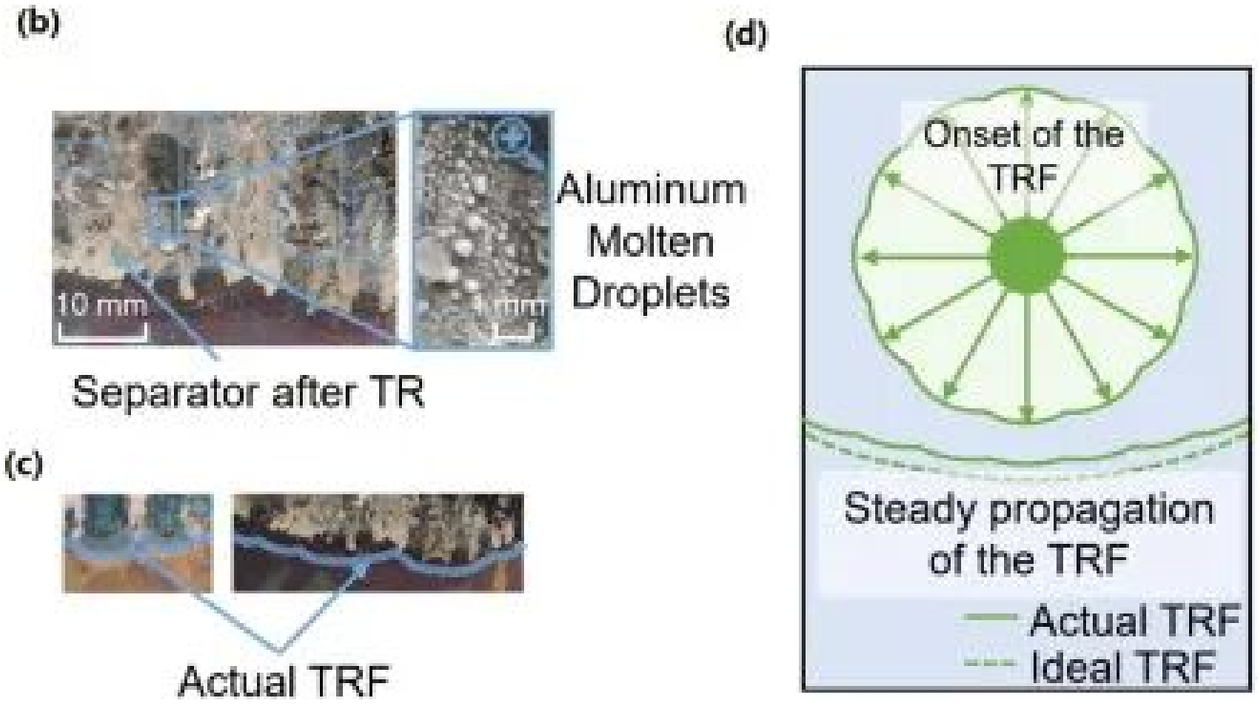

Fig. 6. Optical morphology and shape of the TRF.

1.3.3 Micro-CT Analysis of the TRF (Fig. 7)

1) Structural features of the TRF region

Normal region: In the X-section, the positive-electrode layer is brighter and the negative-electrode layer is darker, while the separator is invisible due to its high X-ray transmittance. Near the TRF, a clear gap appears between the positive and negative electrode layers, indicating that gas generation and thermal expansion during TR have loosened the electrode structure.

TRF transition region: The Y-section spans the TRF; the electrode structure can be observed to gradually transition from an intact state to a completely failed state. This continuous change directly reflects the progressive destruction of the internal electrode structure during TRF propagation.

2) Degradation of the positive-electrode material

Initial bulging: Approaching the TRF, the positive-electrode active material first bulges locally and begins to separate from the aluminum current collector.

Delamination expansion: As TR further develops, the local delamination area keeps expanding, until the positive-electrode active material completely detaches from the current collector. High-temperature binder failure is the main cause; gas flow and thermal expansion further promote separation.

Material fragmentation: After complete TR, the positive-electrode active material severely fractures and breaks into many small fragments; some positive-electrode fragments further adhere to the negative-electrode surface.

3) Current-collector melting and interfacial reaction

Al current-collector melting: In the fully TR region, the aluminum current collector is almost invisible, indicating it may have completely melted. Some molten aluminum forms small droplets that adhere to the negative-electrode surface and may simultaneously participate in the TR reaction.

Direct electrode contact: Detached positive-electrode fragments directly contact the negative electrode, significantly shortening the mass-transport distance. This may enhance local thermochemical reactions and heat release through direct interfacial reactions and short-range gas-phase mass transfer.

4) Physical failure mechanisms inside the TRF

Evolution path: positive-electrode bulging → local delamination → complete delamination → active-material fragmentation → aluminum current-collector melting.

Propagation features: The TRF is not simply a temperature-propagation boundary, but a complex reaction region where electrode delamination, fragmentation, melting, and interfacial reconstruction continuously occur.

Method limitation: Micro-CT mainly provides internal morphology and structural information; specific chemical reactions and their pathways still cannot be confirmed solely from CT results.

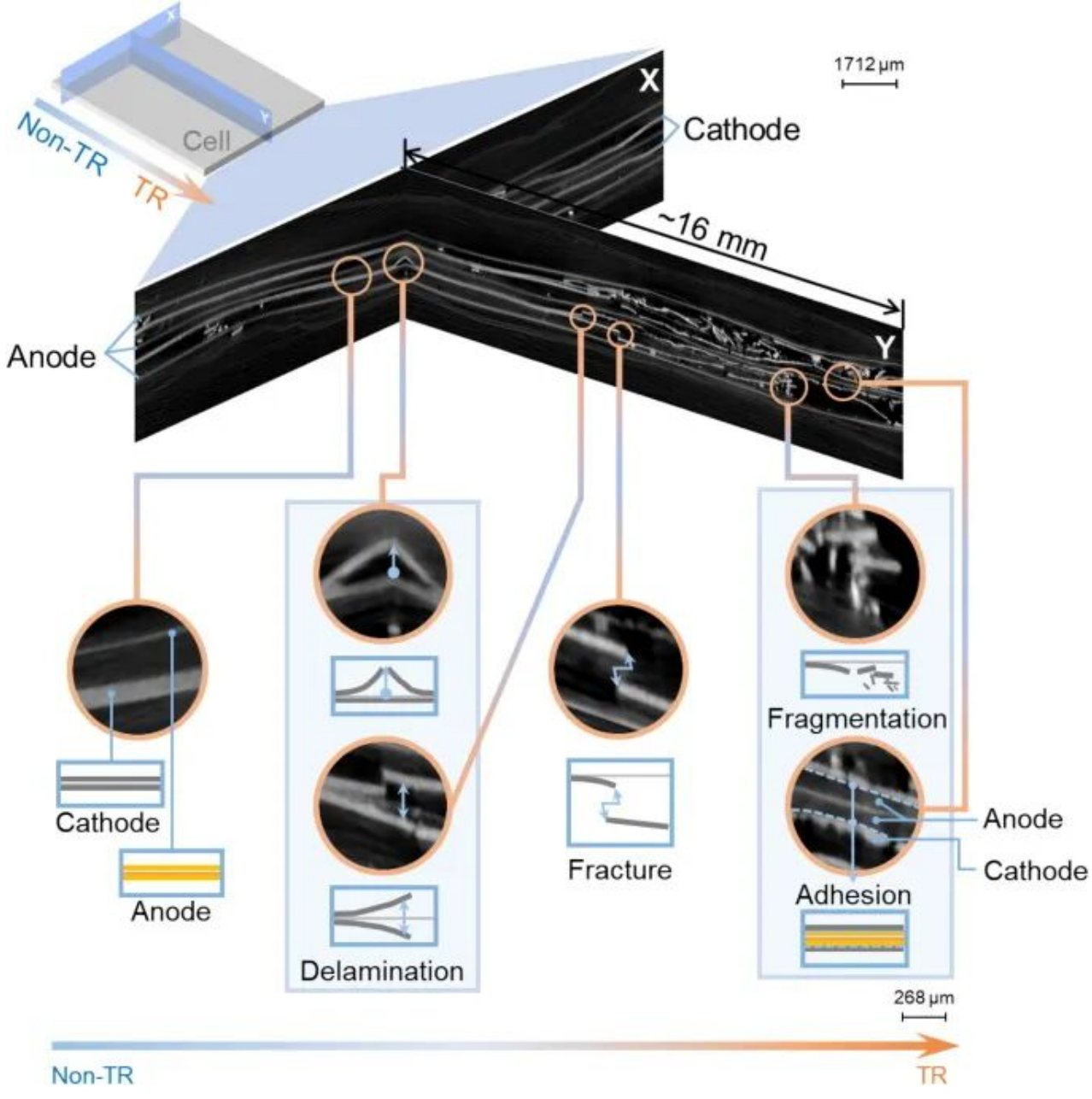

Fig. 7. CT scan results of cell debris containing the TRF

1.3.4 TRF-Induced Material Failure Mechanisms (Fig. 8)

1) Preferential separator failure

Thermal triggering: As the TRF advances, heat from the TR region is first transferred to the separator ahead, so the separator undergoes physical failure first. The PP/PE separator matrix begins to decompose at about 130–150 °C.

Morphological evolution: The separator gradually changes from its original state to transparent, then to a scorched yellow-brown. Because a ceramic coating is present, the separator does not show obvious large-scale thermal shrinkage.

Residual ceramic layer: After the PP/PE matrix fully decomposes, the high-temperature-resistant ceramic coating remains, mainly adhering to the negative-electrode surface.

2) Delamination and fragmentation of positive-electrode active material

Binder failure:When the temperature rises to about 400–450 °C, the positive-electrode binder decomposes. The bonding strength between active material and aluminum current collector drops significantly, and delamination begins.

Electrode delamination: The positive-electrode active material gradually detaches from the aluminum current collector; some detached positive material further adheres to the negative-electrode surface.

Material fragmentation: Gas release and thermal expansion from TR further promote fracture of the positive material; the remaining material ultimately forms irregular fragments dispersed in the cell debris.

3) Aluminum current-collector melting and corrosion

High-temperature melting: The aluminum current collector begins to melt at about 660 °C. Numerous corrosion pits simultaneously appear on its surface, indicating significant high-temperature damage.

Molten-aluminum migration: After complete melting, some aluminum forms molten droplets that further adhere to the surface of the residual ceramic coating.

Potential chemical reactions: Some unobservable aluminum current collector may not only melt but also participate in TR chemistry. Molten aluminum may undergo aluminothermic-like reactions with metal oxides or reduced metals produced by the positive electrode, further enhancing local heat release.

4) Continuous failure path induced by the TRF

Progressive material failure path

Low temp. PP/PE separator matrix decomposes → separator functional failure → localized internal short circuit → **Mid temp**. Positive-electrode binder decomposes → active-material delamination, fracture, fragmentation → **High temp**. Al current collector corrodes & melts, possibly entering high-temperature thermochemical reactions.

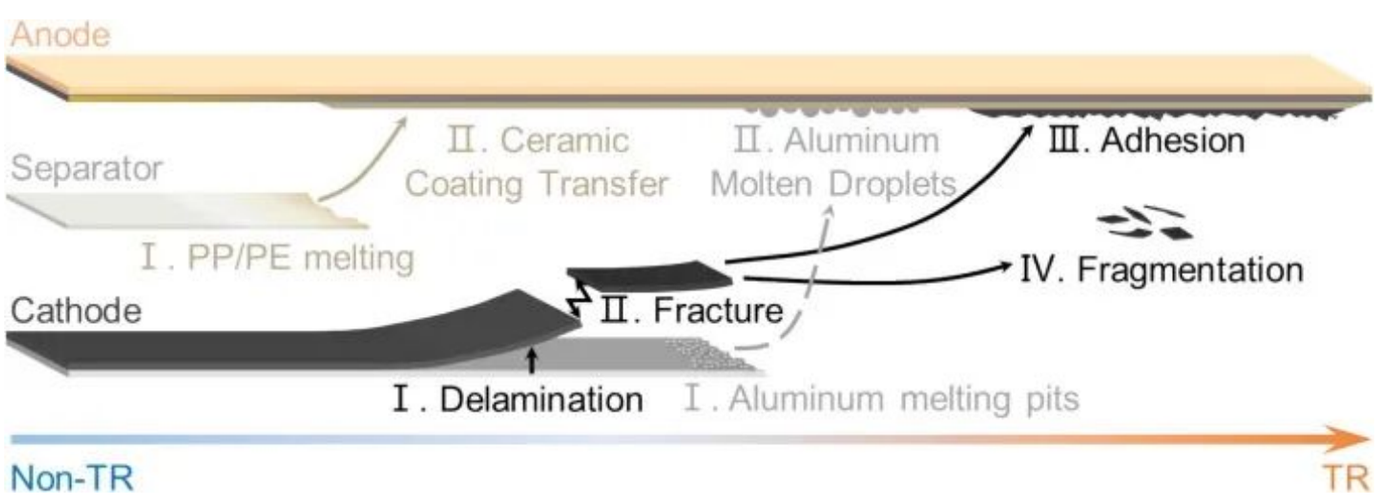

Fig. 8. Mechanistic insights into the physical failure processes at the TRF in lithium-ion batteries.

1.3.5 Significance of the TRF Cryo-Arrest Method (Fig. 9)

Preserving the transient TRF: Cryogenic freezing can rapidly terminate TRF propagation before the entire cell undergoes complete thermal runaway, preserving centimeter-scale spatial reaction structures. The frozen TRF can be regarded as a spatial projection of the rapid T1–T3 reaction process, used to track local material-failure evolution.

Spatial chemical characterization: Compared with DSC, ARC, TG and MS, this method yields spatially resolved samples at different TRF positions. It can be combined with SEM, XRD, XPS and EDS to analyze local morphology, phase composition, surface chemical states and element migration, reconstructing the sequence of TRF reactions and material degradation.

Advantages & limitations:This method overcomes the limits of in-situ TEM/XRD in sample size, compositional integrity and heating conditions. The 1 mm reconstructed cell differs from commercial pouch cells in heat transfer, gas accumulation and mechanical constraints, so results mainly reveal local failure mechanisms and should not be directly extrapolated to quantitative propagation characteristics.

Mechanistic research potential: The frozen TRF can also analyze TR-regulation mechanisms such as radical trapping and thermally triggered microcapsules and their spatial effects. Thus the method is both a TRF-arrest means and an important approach for preserving and reconstructing the spatial sequence of chemical reactions and material degradation during TR.

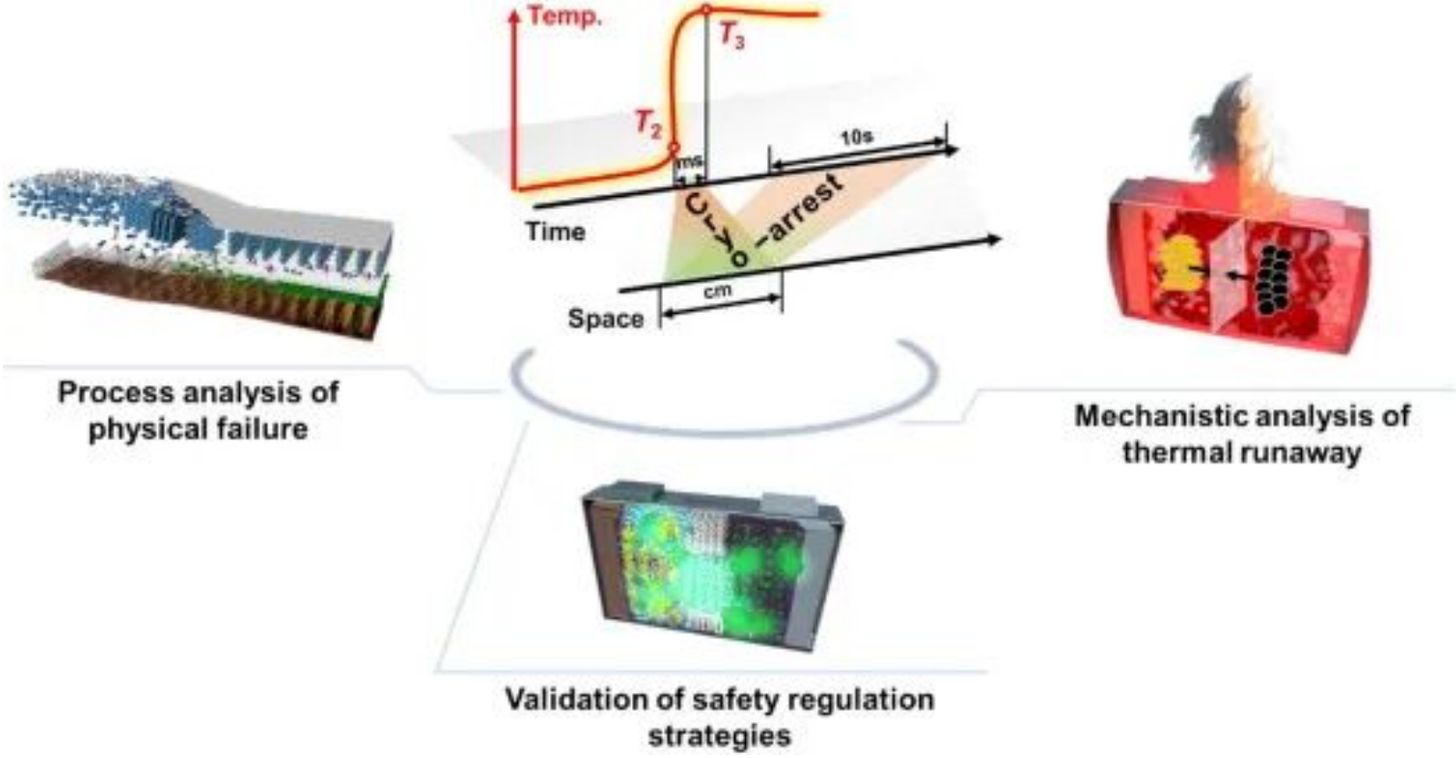

Fig. 9. Potential applications of the TRF cryo-arrest method.

Conclusions

Good reproducibility of cryogenic arrest. The TRF ultimately stops between TC4 and TC5; the mean arrest distance over 15 experiments is 0.1637m with a CV of13.6%, indicating that liquid-nitrogen cryo-arrest can stably control the TRF stopping position.

The TRF exhibits multi-front superimposed propagation. The TRF width is about 10 mm, evolving from "local initiation → superposition of multiple arc-shaped fronts → front merging → stable arc-shaped propagation," rather than always propagating as a single front. Separator failure near the TRF induces localized internal short circuits; short-circuit heat is an important driving force sustaining TRF propagation

The TRF corresponds to progressive internal structural destruction. Micro-CT shows the TRF region gradually transitions from intact electrodes to a completely failed state: "positive-electrode bulging → local delamination → complete delamination → active-material fragmentation → aluminum current-collector melting."

Material failure shows a clear temperature sequence.130–150 °C — PP/PE separator decomposes first; 400–450 °C — positive-electrode binder fails, causing active-material delamination and fragmentation; ≈660 °C — aluminum current collector melts and may participate in further high-temperature thermochemical reactions.

Cryo-arrest spatially freezes the transient TRF structure. The method not only arrests the TRF but also preserves the spatial state of the rapid T1–T3 process, and combines SEM, XRD, XPS, EDS to reconstruct the internal material-degradation and potential chemical-reaction sequences of the TRF.

1. Original Paper Link： https://doi.org/10.1016/j.jechem.2026.07.094

2. Corresponding Author

Google Scholar: scholar.google.com/citations?user=oIjjYG0AAAAJ

ScienceDirect: sciencedirect.com/author/55084333300

University Web: svm.tsinghua.edu.cn/essay/74/1837.html

PREV IN COLLECTION
Cell-level TR Propagation Series

NEXT
Comments on Simulation Study